INTERNATIONAL JOURNAL OF INTEGRATED ENGINEERING
ISSN: 2229-838X e-ISSN: 2600-7916

IJIE

Vol. 17 No. 6 (2025) 58-70
https://publisher.uthm.edu.my/ojs/index.php/ijie

A Compact and Efficient U-Slot Excited Substrate Integrated Waveguide-Based Antenna for 5G-NR Millimeter Wave Band

Nida Nasir[1,2]*, Mohd Haizal Jamaluddin[1]*, Nor Hidayu Shahadan[3], Noor Azwan Shairi[4]

[1] *Wireless Communication Centre, Faculty of Electrical Engineering, Universiti Teknologi Malaysia, Johor, MALAYSIA*
[2] *Faculty of Telecommunication Engineering, NED University of Engineering and Technology, 75270, Karachi, PAKISTAN*
[3] *Electrical Engineering Department, Politeknik Ibrahim Sultan. Pasir Gudang, Johor, MALAYSIA*
[4] *Fakulti Teknologi dan Kejuruteraan Elektronik dan Komputer (FTKEK), Universiti Teknikal Malaysia Melaka (UTEM), Melaka, MALAYSIA*

*Corresponding Author: haizal@utm.my, nida@graduate.utm.my
DOI: https://doi.org/10.30880/ijie.2025.17.06.005

Article Info

Received: 14 March 2025
Accepted: 28 October 2025
Available online: 30 December 2025

Keywords

5G-NR, U-slot, broadband, higher order mode, millimeter (mm) wave, cubical dielectric resonator antenna (CubDRA), substrate integrated waveguide (SIW)

Abstract

In the article, a cubical dielectric resonator antenna is excited through a U-slot aperture utilizing a Substrate Integrated Waveguide feeding mechanism. This antenna works in three different frequency bands of the millimeter range, 25.8, 27.5, and 30.4 GHz, targeting the 5G-NR bands, N257, and N258. The simulated antenna produces a substantial bandwidth of 6.12 GHz (25-31.12 GHz), a peak elevated gain of 8.9 dBi with 98% efficiency. The radiation patterns indicate the absence of backside radiation, validating the broadside transmission of the proposed antenna. All simulations for antenna design were carried out using Ansys HFSS, confirming the antenna's suitability for high-performance 5G wireless communication systems, including applications in indoor environments, IoT infrastructure, and smart mobility platforms.

1. Introduction

As 5G technology progresses [1] antenna designers are working on developing a high-gain antenna with a large bandwidth and low loss to compensate for propagation losses during signal transmission and reception. Various design solutions have been proposed for the 5G mmwave band (n257: 26.5 GHz to 29.5 GHz, and n258: 24.25 GHz to 27.5 GHz) [2]. Conventional single antennas usually offer low gain (below 6 dBi), which is inadequate for real-world use. To overcome this, multi-element systems like phased arrays and multiple input multiple output (MIMO) are explored to boost gain and directivity, though they come with increased design challenges. Microstrip patch antennas (MPA) are popular radiating elements because of their light weight and low fabrication cost, but they suffer from losses resulting in narrow bandwidth, limited gain, and lower efficiency. At mmwave frequencies, the losses in MPA become predominant, so these limitations can be covered by realizing the use of dielectric as a resonator. These dielectric resonators are gaining popularity because of their wide bandwidth, high gain, and higher efficiency. Dielectric resonator antennas (DRA) can be excited through different feeding techniques such as microstrip line, coaxial, aperture/slot, conformal feed, and more. Recently, Substrate integrated waveguide (SIW) has been used as a low-loss feeding structure as a replacement for heavy waveguides and lossy microstrip lines [3]. It is created by two periodic rows of metallic vias that connect the top and bottom of the planes [4]. The bandwidth and gain performance of DRA can be improved through different approaches, such as combining

different DR, creating perforations/drilling holes, DR separated by an air gap or foam, modifying the shape of DR, multiple substrates, stacked DRA, hybrid DRA, parasitic elements, and more [5-9].

Various reported antennas in literature at the designed frequency are discussed herewith: [10] presents an SIW cavity-based U slot using a patch antenna, which has a bandwidth from 26.20–30.30 GHz (14.51%) and a peak gain of 7.5 dBi and a radiation efficiency of 91.29%. In [11] a bowtie antenna is fed by a microstrip line (ML) utilizing a defective ground structure, has a bandwidth of 26.7 to 28.7 GHz, and a 2-element array with a peak gain of 12 dBi and a bandwidth of 27 to 30 GHz. The antenna resonates at three bands covering 28, 35, and 38 GHz, 5G bands in [12] proposed dielectric antenna has a stacked radiator with semi-circular slots etched on the left and right sides of an upper radiator, excited through ML, having a maximum radiation efficiency of 97.63%, and a maximum gain of 7.6 dBi is noted. [13] utilizes perforated DRA and a metal strip with SIW feeding, resulting in bandwidth from 24.4 to 32.6 GHz, peak gain of 7.4dBi, and efficiency above 90%. The antenna in [14] is composed of a cylindrical dielectric resonator and a truncated plastic-based conical horn is excited by a slot/aperture feed, resulting in a bandwidth of 13.6% (27.7 and 32.7 GHz) with a peak realized gain of 12.6 dBi. A very wide aperture with SIW feed and DRA with top-loaded patch is reported in [15], resulting in a 40% impedance bandwidth spanning from 25 to 38 GHz with a peak gain of 7.1 dBi. [16] A triple-band cavity-backed substrate integrated waveguide (SIW) based slot antenna stacked with the metasurface operating in the millimeter-wave region is proposed yields three bands, 22.389 GHz to 23.562 GHz (5%), 29.73 GHz to 30.239 GHz (1.69%), and 36.105 GHz to 38.968 GHz (7.62%). The maximum radiation efficiencies are 88.37%, 88.63%, and 89.85%, peak gains in the three operating bands are 7 dBi, 8.5 dBi, and 14.5 dBi in the operating bands of 22.389 GHz to 23.562 GHz, 29.73 GHz to 30.239 GHz, and 36.105 GHz to 38.968 GHz, respectively.

The primary objective of this paper is to provide a one-window solution through the use of a dielectric as a resonating element, which has the benefits such as no copper losses, a wide bandwidth, and high efficiency. In addition, it supports higher gain when higher modes are excited. The feeding through the SIW [17] provides better overall efficiency while integrating the merits of the waveguide and planar technology to provide a lightweight and low-loss structure. The suggested antenna employs a substrate integrated waveguide feed deploying a cubical DRA forming an efficient radiating structure. Accordingly, DRA is energized by a U-shaped slot etched on the top metallization of the SIW. This design targets 5G-NR applications, aiming to achieve broad impedance bandwidth, reduced losses, improved radiation efficiency, and elevated gain, all within a compact, low-profile single-element architecture.

2. Antenna Design

This paper presents the design and implementation of a broadband substrate integrated waveguide (SIW)-fed dielectric resonator antenna (DRA) with a U-slot aperture coupling for 5G applications. The proposed antenna leverages the advantages of SIW technology, including its compact size, low cost, and ease of integration, combined with the high Q-factor and wide bandwidth characteristics of DRAs. Firstly, a two-port SIW is designed and analysed for proper function. Thereafter, a U-shaped slot is strategically placed on the ground plane of the SIW, providing a pathway for electromagnetic energy to couple from the SIW waveguide to the DRA, ensuring maximum power transfer as in Fig. 1. The dimensions and placement are carefully optimized to enhance the antenna's impedance matching and bandwidth performance. The feeding mechanism of the proposed antenna involves a substrate integrated waveguide (SIW) that acts as a transmission line for the electromagnetic signal.

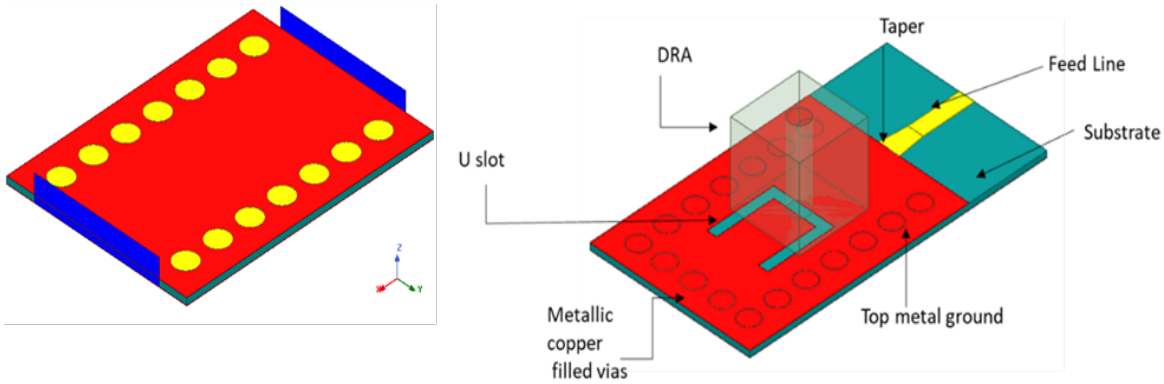

Fig. 1 *SIW Antenna design (a) two port; (b) DRA with a U slot and tapered transition line*

2.1 Design of Substrate Integrated Waveguide (SIW)

Substrate-integrated waveguides (SIW) exhibit propagation and dispersion characteristics like rectangular waveguides. Due to the presence of gaps between adjacent vias, transverse magnetic (TM) modes are not supported; therefore, only transverse electric (TE $_{n0}$) modes exist. To build an SIW structure, three important parameters are obtained, i.e., the width of the SIW a_{siw}, metalized via diameter d_{via}, and the distance between two vias p. Generally, the width of SIW, a_{siw} is smaller than the width of the waveguide, a, because of the existence of the dielectric substrate having permittivity ε_{rs}. The design equation for SIW is mentioned below [18].

SIW cutoff frequency

$$f_c = \frac{c}{2a} \tag{1}$$

Dielectric Filled Waveguide (DFW) width

$$a_d = \frac{a}{\sqrt{\varepsilon_{rs}}} \tag{2}$$

SIW width

$$a_{siw} = a_d + \frac{{d_{via}}^2}{0.95p} \tag{3}$$

Guided wavelength

$$\lambda_{g_{SIW}} = \frac{\lambda_0}{\sqrt{\varepsilon_{rs}\left[1 - \left(\frac{f_c}{f_0}\right)^2\right]}} \tag{4}$$

Necessary conditions for SIW are as follows

$$d_{via} = \frac{\lambda_{g_{SIW}}}{5} \; ; \; p < 2\, d_{via} \tag{5}$$

2.2 Design of Dielectric Resonator Antenna (DRA)

The resonating material used here is a dielectric with a permittivity ε_{rd}. The dielectric waveguide model (DWM) is used for determining the resonant frequency f_o of the cubical DRA with k_o , k_x , k_y , k_z are the wave numbers along the free space, x, y, and z directions, respectively. The length, width, and height of DRA are denoted by L_d, W_d, and H_d [19].

$$k_y \tan(k_y W_d/2) = \sqrt{(\varepsilon_{rd} - 1)\, {k_o}^2 - {k_y}^2} \tag{6}$$

$${k_x}^2 + {k_y}^2 + {k_z}^2 = \varepsilon_{rd}\, {k_o}^2 \tag{7}$$

$$k_x = \frac{\pi}{L_d}; \; k_z = \frac{\pi}{2H_d}; \; k_o = \frac{2\pi f_o}{c} \tag{8}$$

3. Design Methodology

3.1 SIW Working

Initially, a comprehensive study was conducted to determine the optimal dimensions of the Substrate Integrated Waveguide (SIW) structure, considering a two-port configuration (input and output ports). The plots in Fig. 2 shows the complex propagation constant (γ), gamma plot versus cutoff frequency. In this context, the imaginary part of γ corresponds to the phase constant (β), while the real part represents the attenuation constant (α). Both components are essential in identifying the cutoff frequencies of supported modes within the SIW structure. Likewise, the cutoff frequency in a waveguide is inversely proportional to the width as well as the permittivity of the substrate $f_c \propto 1/\varepsilon_{rs}$. Accordingly, the effective operating range of the SIW is typically bounded between 1.25 f_c to 1.9 f_c which in this case spans from (22 to 32 GHz). Given that the proposed antenna is intended to operate within the 5G-NR frequency bands N257/N258 (24.25–29.5 GHz), the design is aligned with this operational range. As illustrated in Fig. 2a the computed cutoff frequency for the TE_{10} is 17.34 GHz, whereas the resonance frequency begins at 22 GHz for an SIW width a_{siw} of 5.8 mm as shown in Fig. 2b. Due to symmetry, the S-parameter plots display identical results for reflection coefficients S_{11} and S_{22}, similarly for transmission

coefficients S_{21} and S_{12}. The symmetry is also reflected in the gamma plots for real and imaginary components. The reflection coefficient (S_{11} and S_{22}) quantify the power reflected back from each port, while the transmission coefficients (S_{21} and S_{12}) indicate the isolation or power transferred between ports. These parameters confirm proper wave propagation and minimal reflection loss across the waveguide section.

The SIW electric field plots show the working of a waveguide, with the field intensity shown in Fig. 3 and Fig. 4 further validate the TE_{10} mode excitation. Simulations at 24, 26, 28, and 30 GHz reveal strong field confinement within the SIW cavity bounded by the metallic via walls, with negligible leakage. The color intensity represents the field magnitude, where red denotes high field strength and blue indicates weaker regions. The field patterns confirm that the SIW structure supports dominant-mode propagation with efficient energy confinement, forming a reliable transition interface for DRA excitation in the proposed antenna.

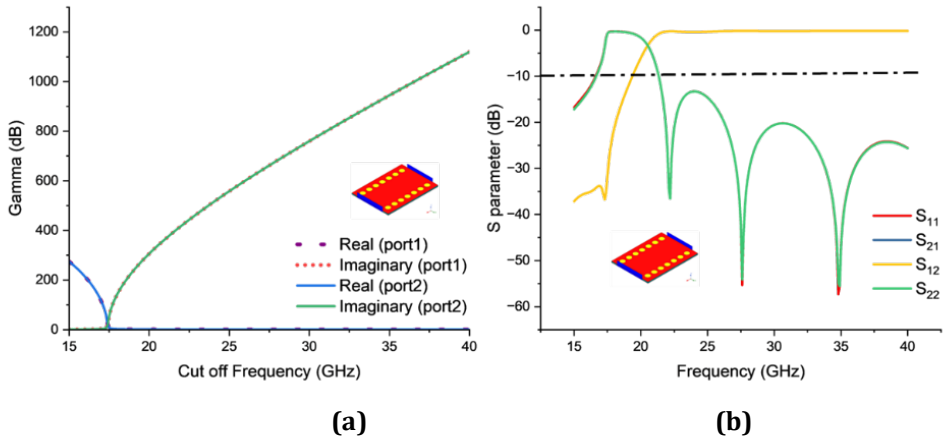

Fig. 2 *SIW design (a) gamma vs cutoff frequency; and (b) S-parameter versus resonant frequency plot*

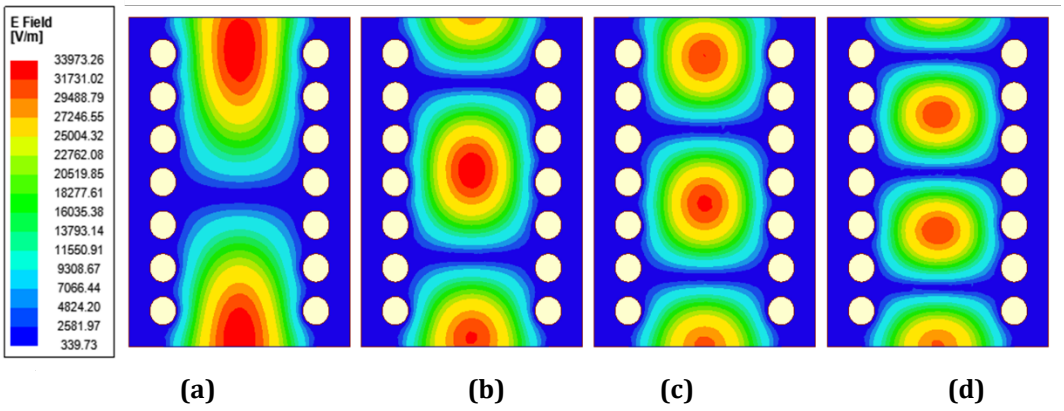

Fig. 3 *SIW E field magnitude plot (TE_{10}) at frequencies (a) 24 GHz; (b) 26 GHz; (c) 28 GHz; and (d) 30 GHz*

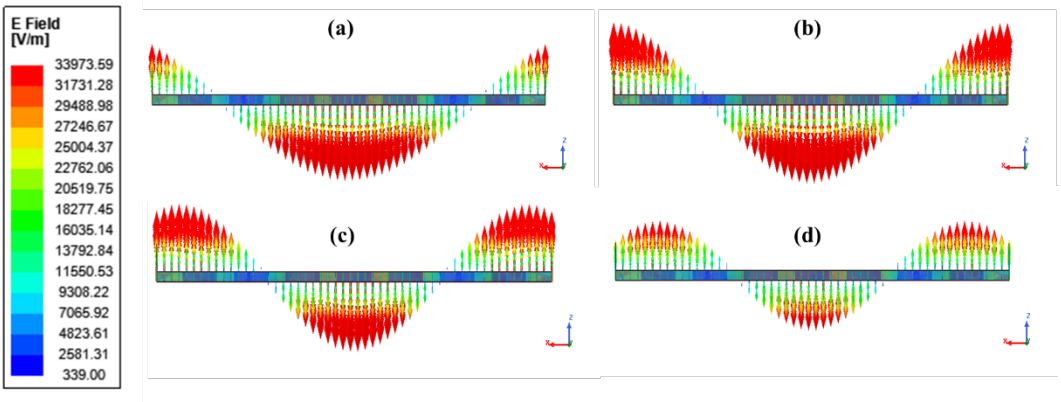

Fig. 4 *SIW E field vector plot at (TE_{10}) frequencies (a) 24 GHz; (b) 26 GHz; (c) 28 GHz; and (d) 30 GHz*

Int. Journal of Integrated Engineering Vol. 17 No. 6 (2025) p. 58-70

The frequency in SIW mainly depends on the width of the waveguide and the diameter of the vias, so a parametric study is carried out to see the change in frequency values with the change in a_{siw}, and d_{via}. The relation between the via diameter and with S parameter and the gamma plot is displayed in Fig. 5a and b. As the via diameter increases, the resonant frequency shifts towards the higher side. The propagation constant is independent of the impact of the via diameter, therefore if d_{via} changes, no change is observed in the plot as in Fig. 5b. Furthermore, the relation between the SIW width with S parameter and gamma plot is presented in Fig. 6. As the width a_{siw} is increased, the resonant frequency shifts towards the lower side. In addition, the gamma plot displays a similar trend, i.e, the higher the SIW width, the lower the cutoff frequency, verifying the inverse relationship between the cutoff frequency and SIW width. Since the targeted resonant frequency is above 24 GHz, therefore, after carrying out the parametric study for SIW diameter and SIW width, the chosen values for d_{via}. is 1 mm and a_{siw} is 5.8 mm, respectively.

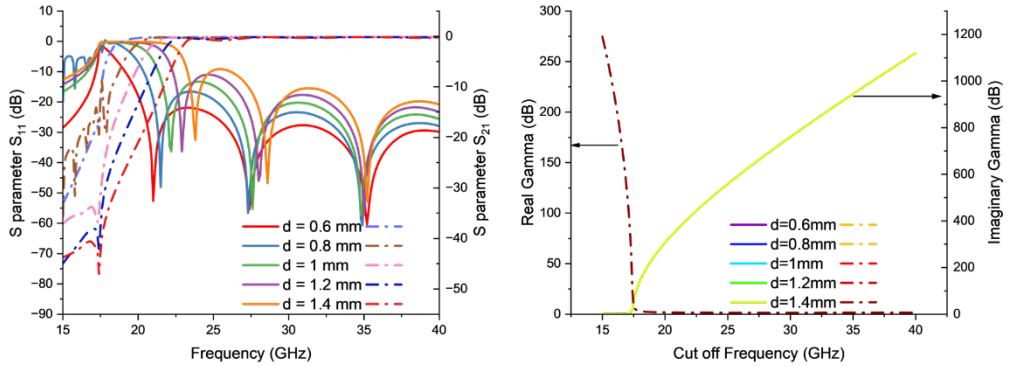

(a) **(b)**

Fig. 5 *Parametric study for via diameter (a) S parameter plot; (b) Gamma plot*

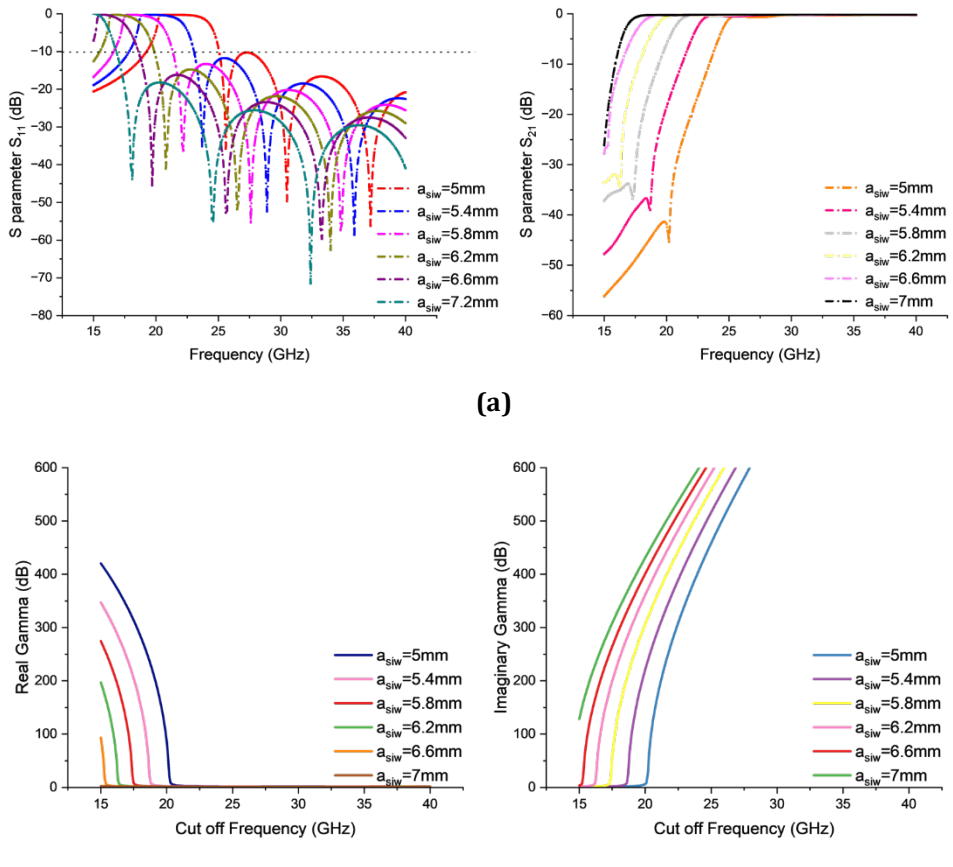

(a)

(b)

Fig. 6 *Parametric study for SIW width (a) S parameter plot; (b) Gamma plot*

3.2 SIW-DRA Working

The SIW is clad with 0.035 mm copper on both sides of Rogers substrate 5880, whose permittivity is 2.2. The rectangular waveguide (WR34) is taken as a reference for designing the substrate integrated waveguide. The DRA is in cubical shape with dimensions of 3.6x3.6x3.6 mm^3, has a permittivity of 10. The design parameters for both the SIW and DRA are discussed in Sections 2.1 and 2.2, respectively. The SIW is designed first thereafter the transition was created following the different slot orientations. The process of design steps of the antenna are illustrated in Fig. 7.

The slots are created on top of the metal surface of a substrate. At stage 1, a longitudinal slot of dimensions of length 3 mm and width 0.5 mm is proposed. Later, at the second stage, the slot is modified as an L slot by adding a transverse slot at the end, having a slot length of 3.2 mm and a width of 0.5 mm. Thereafter, a U slot is created utilizing a slot length of 3 mm and 3.2 mm, whereas the width of 0.5 mm remains unchanged for both slots. In all cases, the perforated DRA is loaded on the slot for proper coupling. Fig. 8 displays the top view and side view of the final design antenna. Furthermore, Table 1 highlights the optimized dimensions of the U-slot SIW DRA antenna design. The dimensions to analyse the slot values are calculated by 8 (l_s), and 9 (w_s) [20]:

$$l_s = \frac{0.4\,\lambda_0}{\sqrt{\varepsilon_{reff}}}; \qquad \varepsilon_{reff} = \frac{Heff}{\frac{H_d}{\varepsilon_{rd}} + \frac{H_{sub}}{\varepsilon_{rs}}}; \qquad H_{eff} = H_d + H_{sub} \tag{8}$$

$$w_s = 0.2\,L_s \tag{9}$$

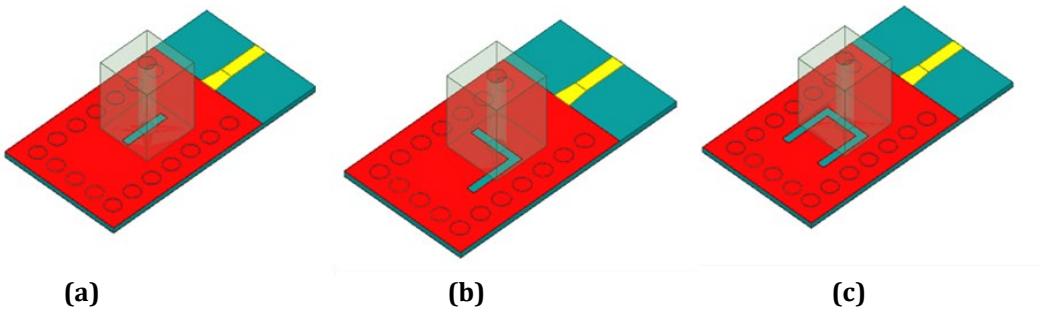

(a) **(b)** **(c)**

Fig. 7 *Progression of preliminary design steps (a) longitudinal (I) slot; (b) L slot; (c) U slot*

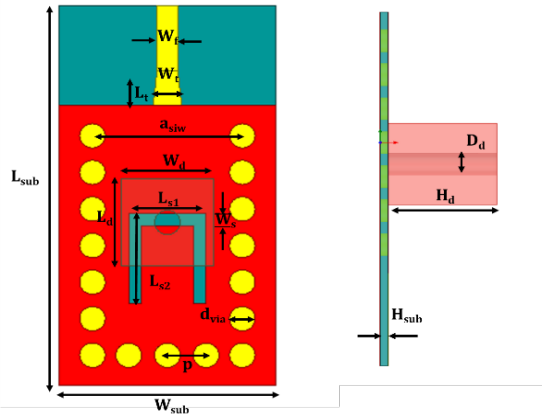

(a) **(b)**

Fig. 8 *Final design (a) Top view; (b) side view*

Int. Journal of Integrated Engineering Vol. 17 No. 6 (2025) p. 58-70

Table 1 *Optimized dimension of U slot SIW DRA antenna design*

Parameter	length (mm)	Width (mm)	Height (mm)
Substrate (L_{sub}, W_{sub}, H_{sub})	15.6	8.4	0.254
Dielectric Resonator Antenna (L_d, W_d, H_d)	3.6	3.6	3.6
Substrate Integrated Waveguide (L_{siw}, a_{siw}, H_{siw})	9	5.8	0.254
Microstrip Feed (L_f, w_f)	2.7	0.8	
Taper (L_t, w_t)	1.4	1.1	
U Slot (l_{s1}, w_{s1}, l_{s2} and w_{s2})	l_{s1}:3.2, l_{s2} :3	w_{s1},w_{s2}:0.5	
Via diameter (d_{via})		1	
Distance between via (p)		1.5	
DRA perforation diameter (D_d)		1 mm	

4. Results and Performance Analysis

In the initial stage featuring a longitudinal slot, the antenna fails to excite adequately due to an impedance mismatch, as evidenced by the S_{11} and gain plots presented in Fig. 9, which indicates a lack of gain for stage 1. In the subsequent stage, impedance matching is successfully achieved, as indicated by the resonant frequencies and corresponding gain values for the L slot. Given that the antenna is engineered for operational frequencies ranging from 24.25 to 29.5 GHz, the performance metrics for the U slot in stage 3 exhibit remarkable outcomes regarding S_{11}, gain, and efficiency. The comparative reflection coefficient plots reveal that the simulated performance of the proposed antenna encompasses a broad frequency range from 25 to 31.12 GHz, maintaining an S_{11} below -35 dB within the specified frequency bands, thereby classifying it as a broadband antenna. Correspondingly, the gain plot highlights the elevated gain values with a peak gain of 9.2 dBi occurring at 26.8 GHz. To further prove the efficacy of the proposed antenna, the impedance plot and efficiency plot are displayed in Fig. 10. Furthermore, the impedance plot confirms the matching at the resonant frequencies with the DRA and U slot to excite the antenna.

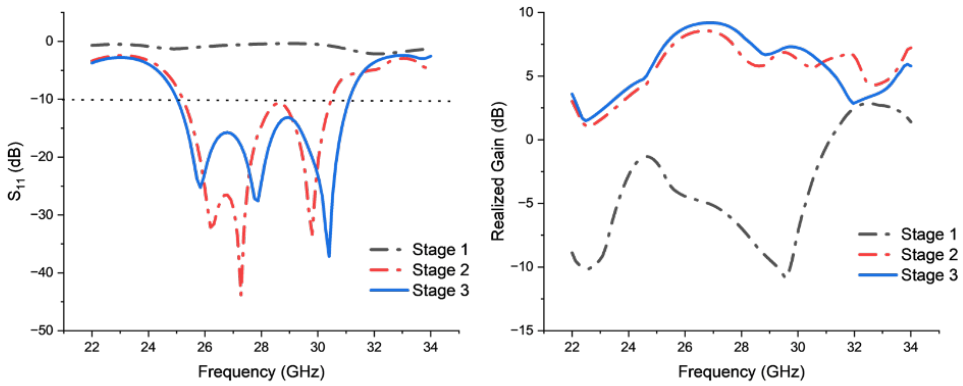

(a) **(b)**

Fig. 9 *Simulated Plot comparison of (a) Reflection coefficient S_{11}; (b) Realized gain*

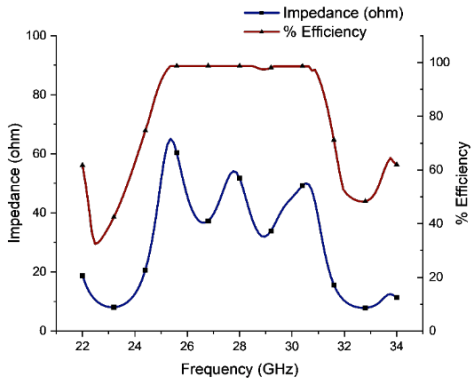

Fig. 10 *Simulated impedance plot, and efficiency*

The simulated two-dimensional (2D) radiation patterns of the proposed antenna are presented in Fig. 11, illustrating the principal E-plane (XY-plane, ϕ = 0°) and H-plane (YZ-plane, ϕ = 90°) responses at the three resonant frequencies of 25.8 GHz, 27.5 GHz, and 30.4 GHz. The patterns exhibit broadside radiation characteristics, with the main lobe directed normal to the antenna surface, indicating effective excitation and radiation from the dielectric resonator via the U-slot–coupled SIW feed.

The half-power beamwidth (HPBW), a critical metric for beam directivity, is observed to vary with frequency. For the E-plane (ϕ = 0°), the HPBW values are 48.3°, 53.2°, and 69.8° at 25.8, 27.5, and 30.4 GHz, respectively. In the H-plane (ϕ = 90°), the corresponding HPBW values are 75.6°, 85.2°, and 98°, indicating a broader beam spread in the H-plane, which is characteristic of many dielectric resonator antennas, possibly due to increased diffraction and reduced electrical size of the resonator at higher frequencies. To further illustrate the three-dimensional (3D) radiation behavior, the 3D polar plots at the resonant frequencies are overlaid in Fig. 12. These plots confirm that the antenna radiates predominantly in the broadside direction (θ ≈ 0°), orthogonal to the ground plane, which is ideal for 5G base station or user equipment applications requiring vertically upward radiation. The antenna achieves peak realized gains of 8.3 dBi at 25.8 GHz, 8.9 dBi at 27.5 GHz, and 6.9 dBi at 30.4 GHz, indicating effective gain performance across the band. The slight decrease in gain at the higher end of the band (30.4 GHz) may be attributed to possible variations in field confinement at higher frequencies.

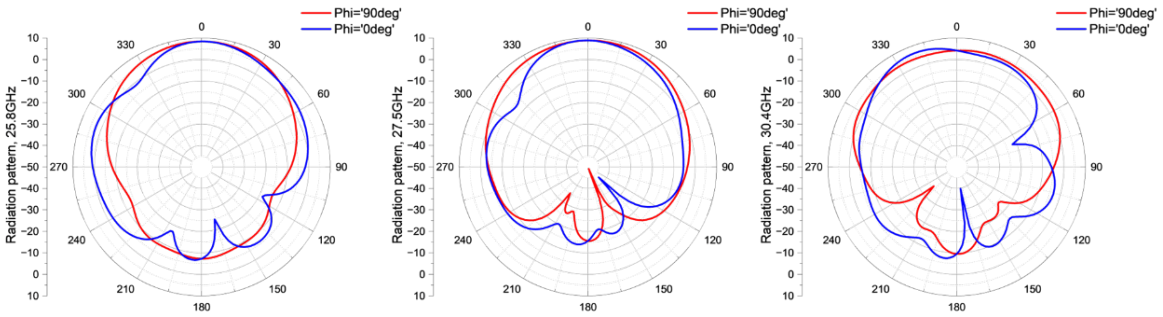

(a) **(b)** **(c)**

Fig. 11 *2D E and H plane simulated radiation plots at resonant frequency (a) 25.8 GHz, (b) 27.5 GHz, (c) 30.4 GHz*

Int. Journal of Integrated Engineering Vol. 17 No. 6 (2025) p. 58-70

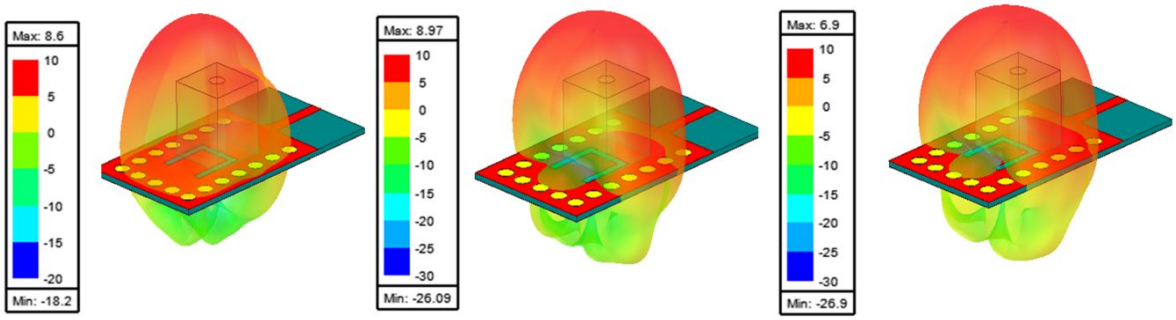

(a) **(b)** **(c)**

Fig. 12 *3D gain plot (a) 25.8 GHz; (b) 27.5 GHz; (c) 30.4 GHz*

To gain insight into the electromagnetic behavior and modal excitation within the dielectric resonator, the electric field distribution inside the DRA was analyzed at the three resonant frequencies of 25.8 GHz, 27.5 GHz, and 30.4 GHz, as illustrated in Fig. 13. The field plots confirm the excitation of higher-order modes, predominantly $TE_{\delta 13}$ and $TE_{\delta 23}$ mode which are characteristic of rectangular or cubical dielectric resonators. These modes are effectively excited by the fringing fields coupled through the U-shaped slot embedded in the SIW top surface, indicating strong coupling between the resonator and the feed structure. At each resonant frequency, the electric field vectors are highly concentrated within the central volume of the DRA, indicating efficient confinement and radiation from the desired mode. The field distribution also confirms that energy is not leaking into the substrate or surrounding region, demonstrating a well-isolated mode profile and strong vertical polarization typical for TE modes.

To complement this, the surface current distribution on the antenna structure is depicted in Fig. 14, providing further verification of the excitation mechanism and radiation behavior. The current density is primarily concentrated around the U-slot region, especially at the slot edges and immediately beneath the DRA, signifying that the slot plays a critical role in exciting the internal resonant modes of the dielectric. The current paths also illustrate effective coupling between the SIW cavity and the dielectric resonator. The color intensity in the surface current plot indicates the magnitude of current density, with the highest concentration observed near the slot-DRA interface. This behavior confirms that the U-slot serves as an efficient aperture, transferring electromagnetic energy from the SIW-fed structure into the resonator. Minimal surface current is observed outside the active region, ensuring low spurious radiation and good radiation efficiency. These field and current distribution analyses collectively verify that the antenna operates in the desired multi-resonant mode regime, with efficient excitation, strong confinement, and minimal leakage, making it well-suited for broadband 5G-NR millimeter-wave applications requiring stable mode control and high radiation efficiency.

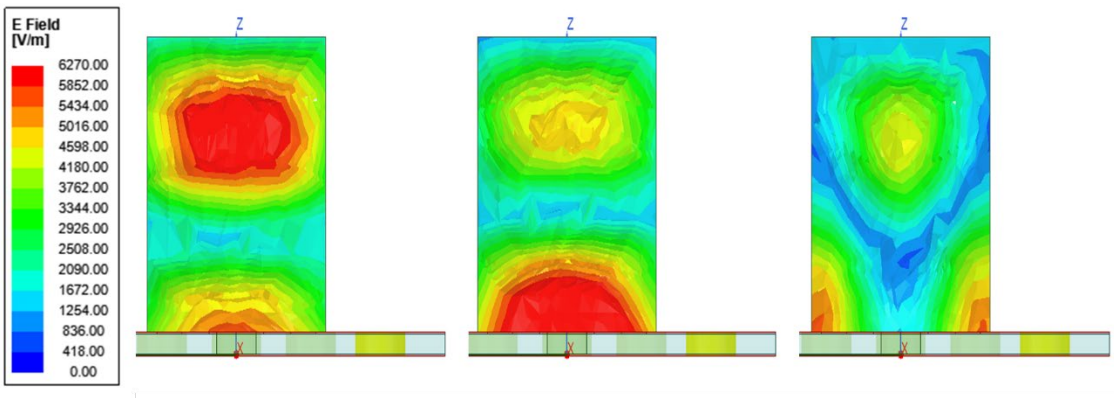

(a) **(b)** **(c)**

Fig. 13 *DRA E-field excitation, (a) 25.8 GHz; (b) 27.5 GHz; (c) 30.4 GHz*

A comprehensive parametric analysis of the proposed SIW-fed dielectric resonator antenna (DRA) was conducted to investigate the influence of the slot dimensions, specifically the slot lengths and widths, on the antenna's impedance matching and resonant behavior. The analysis results are illustrated in Fig. 15. The transverse coupling slot is characterized by its length ls_1 and width ws_1, while the longitudinal slot is defined by ls_2 and ws_2, respectively.

The study reveals that variations in the slot widths (ws_1 and ws_2) significantly impact both the resonant frequency and the impedance matching. As the widths deviate from optimal values, the resonance shifts and mismatch losses increase. However, when equal widths are employed for both transverse and longitudinal slots, specifically at 0.5 mm, a more uniform current distribution is achieved, resulting in improved impedance matching and broader bandwidth. Furthermore, the parametric sweep of slot lengths indicates that shorter lengths (below 2.8 mm) lead to poor matching, likely due to insufficient coupling between the SIW cavity and the dielectric resonator. In contrast, increasing the slot lengths enhances the electromagnetic coupling, which in turn improves impedance bandwidth. Based on these observations, the optimized slot dimensions were determined to be ls_1 = 3.2 mm, ls_2 = 3.0 mm, and ws_1 = ws_2 = 0.5 mm, which yield enhanced impedance characteristics and stable multi-resonant performance across the 5G-NR frequency band.

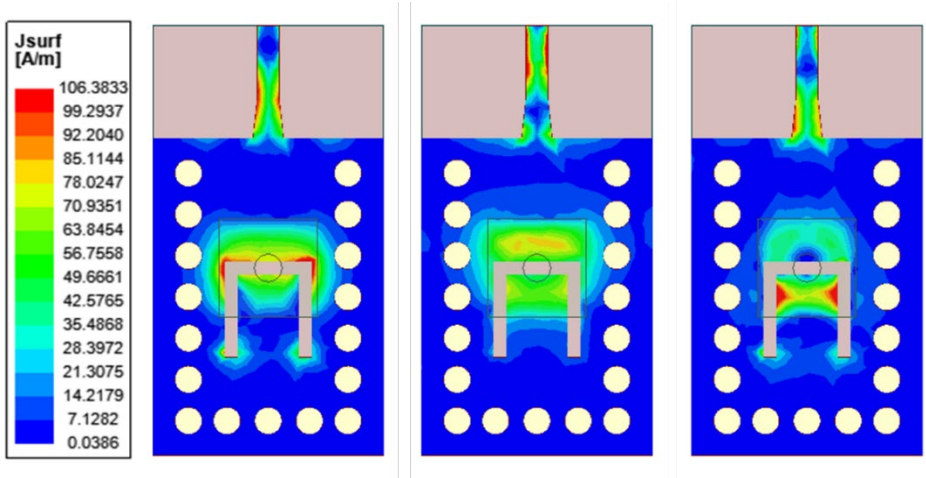

Fig. 14 *Surface current distribution (a) 25.8 GHz; (b) 27.5 GHz; (c) 30.4 GHz*

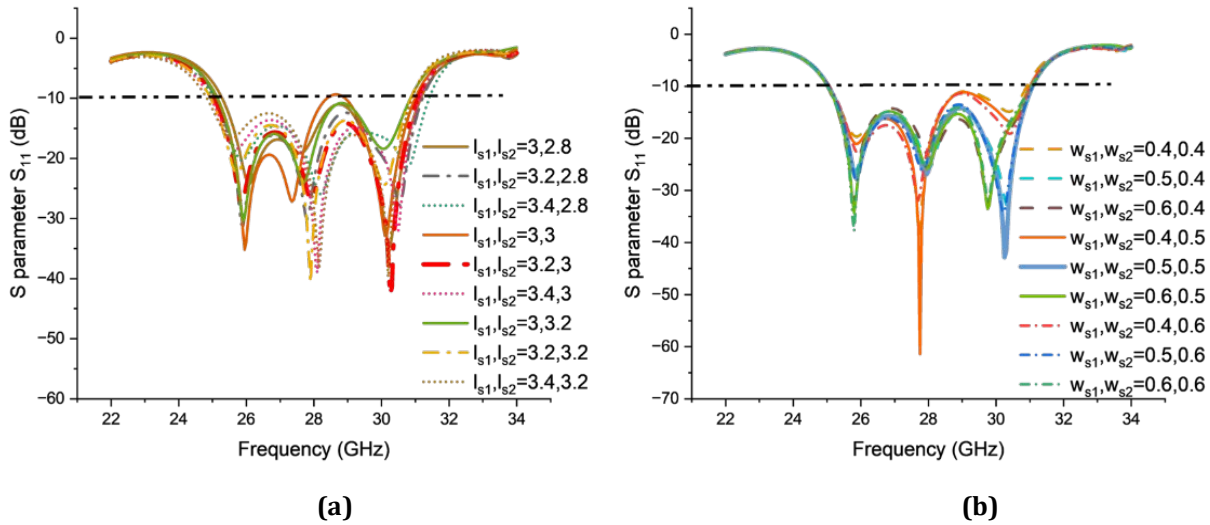

Fig. 15 *Parametric study for U slot (a) Slot length; (b) Slot width*

Table 2 delineates a comparison between the proposed structure and other documented antennas, illustrating that the proposed single element design surpasses the alternatives in terms of bandwidth, gain, and efficiency, specifically within the N257 and N258 bands (26.5–29.5 GHz). Notably, the proposed antenna achieves a realized gain of 8.9 dBi and an impressive impedance bandwidth of 21.8%, covering 25 to 31.12 GHz, with an efficiency of 98%. These metrics collectively outperform several existing designs in the literature. For instance, in [21] a similar SIW-fed microstrip patch antenna with L slots and shorting pins exhibits a moderate gain of 7.5 dBi and a narrower 14.4% bandwidth, albeit with high efficiency (90%). The hybrid antenna in Reference [22] integrates strip, slot, and DRA, offers dual-band operation in 28 and 39 GHz frequency bands but compromises on gain (6.8 and 6.4 dBi)

Int. Journal of Integrated Engineering Vol. 17 No. 6 (2025) p. 58-70

and bandwidth (14.11% and 12.56%). The design in [23] incorporates a stacked patch antenna with a dual metasurface and a U slot, ring slot, achieves a higher gain of 9.3 dBi and wider bandwidth (21.2%) with grounded coplanar waveguide (GCPW) feed, but its complexity and reconfigurable nature may introduce additional fabrication challenges and cost. On the other hand, microstrip-fed antennas such as in [24] utilizes a parasitic planar antenna and reflector elements and [25] a trapezoidal-shaped DRA fed by a microstrip line suffer from lower gain 5.28 dBi and 3.98 dBi respectively, although [19] reports a wide bandwidth (26.3%), it does so at the expense of efficiency and gain. Reference [26] proposes a patch antenna fed by a microstrip line introduces a dual-band with moderate gain (7.8/8.9 dBi), but the bandwidth is significantly narrower (3.34% and 4%), despite high efficiency efficiencies of 96.02% and 95.5% at 28 GHz and 38 GHz, respectively.

Table 2 *Performance of the reported antenna compared with previous work*

Ref	Frequency band	Feeding techniques	Realized Gain dBi	Bandwidth %	Efficiency %
[20],2023	N257, N258	SIW	7.5	14.4%	90
[21],2023	N257, N260	SIW	6.8	14.11%,	NM
			6.4	12.56%	
[22],2024	N257, N258	Metasurface, GCPW	9.3	21.2%	NM
[23],2023	N257, N258	Microstrip	5.28	19.1%	NM
[24],2022	26 GHz	Microstrip	3.98	26.3%	NM
				7.69%	
[25],2025	28/38 GHz	Microstrip	7.8	4%	96
			8.9	3.34%	95.5
Proposed	N257, N258	SIW	8.9	21.8%	98
				(25-31.12) GHz	

NM= not mentioned, GCPW= grounded coplanar waveguide

In contrast, the proposed SIW-fed DRA offers a balanced and optimized trade-off with high gain, broad bandwidth, and excellent efficiency, making it highly suitable for 5G-NR applications requiring stable performance over a wide frequency range. The use of SIW feeding combined with a U-slot coupling mechanism further enhances the broadband behavior while maintaining structural compactness and fabrication simplicity. This establishes the proposed design as a promising candidate in the realm of high-performance 5G mmWave antenna solutions.

5. Conclusion

In this work, a broadband dielectric resonator antenna (DRA) has been proposed and analyzed for millimeter-wave 5G-NR applications, operating at multiple resonant frequencies 25.8 GHz, 27.5 GHz, and 30.4 GHz achieved through multi-mode excitation. The antenna design features a perforated dielectric resonator integrated with a substrate integrated waveguide (SIW) feed, coupled via a U-shaped slot. A comparative performance evaluation was conducted for different slot geometries (I-slot, L-slot, and U-slot), highlighting the U-slot as the most efficient configuration in terms of impedance bandwidth and gain enhancement. The full-wave electromagnetic simulations, performed using ANSYS HFSS, reveal that the proposed configuration achieves a broad impedance bandwidth of 6.12 GHz (21.8%), covering the 25–31.12 GHz range, which fully encompasses the 5G-NR bands N257 and N258. The antenna exhibits a peak realized gain of 8.9 dBi and an efficiency exceeding 98%, with a broadside radiation pattern across the operating band, confirming its suitability for high-directivity wireless systems. In future work, the antenna will be fabricated and experimentally validated to corroborate the simulation results. Measured results will be used to assess fabrication tolerances, evaluate real-world performance, and further optimize the design for practical deployment. The proposed antenna demonstrates a promising balance between bandwidth, gain, and radiation efficiency, attributed to the optimized U-slot coupling mechanism and effective mode excitation within the DRA. The design is compact, planar-integrated, and suitable for mass production, which makes it a strong candidate for implementation in emerging 5G-enabled technologies, including mobile communication, Internet of Things (IoT), and indoor wireless infrastructure such as airports, transport terminals, hotels, shopping malls and commercial spaces.

Acknowledgment

This research work was supported by the HiCoE Grant (Vot 4J618) and UTM Matching Grant (Vot 04M470) both awarded by the Ministry of Higher Education of Malaysia.

Conflict of Interest

The authors declare that there is no conflict of interest regarding the publication of the paper.

Author Contribution

The authors confirm contribution to the paper as follows: ***study conception and design, data collection, analysis and interpretation of results, draft manuscript preparation:*** *Nida Nasir;* ***manuscript checking and proofreading:*** *Mohd Haizal Bin Jamaluddin, Nor Hidayu Shahadan, Noor Azwan, Shairi. All authors reviewed the results and approved the final version of the manuscript.*

References

[1] T. Nahar and S. Rawat, "A Review of Design Consideration, Challenges and Technologies Used in 5G Antennas," *Wireless Personal Communications,* vol. 129, no. 3, pp. 1585-1621, 2023/04/01 2023, doi: 10.1007/s11277-023-10193-x.

[2] M. Pant and L. Malviya, "Design, developments, and applications of 5G antennas: a review," *International journal of microwave and wireless technologies,* vol. 15, no. 1, pp. 156-182, 2023.

[3] J. S. Darling, V. Guruviah, and R. P. Dwivedi, "SIW Technology for 5G Antenna Applications and Beyond—A Critical Review," *International Journal of Communication Systems,* vol. 38, no. 2, p. e6036, 2025.

[4] N. Nasir, M. H. Jamaluddin, and N. H. Shahadan, "A broadband substrate integrated waveguide fed dielectric resonator antenna with U-slot for 5G-NR Band," *Journal of Physics: Conference Series,* vol. 2922, no. 1, p. 012006, 2024/12/01 2024, doi: 10.1088/1742-6596/2922/1/012006.

[5] M. F. M. Omar *et al.*, "A critical review on the development of multi-geometrical stacked wideband dielectric resonator antenna," *Alexandria Engineering Journal,* vol. 100, pp. 111-141, 2024/08/01/ 2024, doi: https://doi.org/10.1016/j.aej.2024.05.028.

[6] M. Shehbaz, C. Du, D. Zhou, S. Xia, and Z. Xu, "Recent progress in dielectric resonator antenna: Materials, designs, fabrications, and their performance," *Applied Physics Reviews,* vol. 10, no. 2, 2023, doi: 10.1063/5.0128779.

[7] M. Abedian, H. Oraizi, S. K. Abdul Rahim, S. Danesh, M. R. Ramli, and M. H. Jamaluddin, "Wideband rectangular dielectric resonator antenna for low-profile applications," *IET Microwaves, Antennas & Propagation,* vol. 12, no. 1, pp. 115-119, 2018, doi: https://doi.org/10.1049/iet-map.2017.0593.

[8] H. Yon *et al.*, "Development of C-Shaped Parasitic MIMO Antennas for Mutual Coupling Reduction," *Electronics,* vol. 10, no. 19, p. 2431, 2021. [Online]. Available: https://www.mdpi.com/2079-9292/10/19/2431.

[9] Yon, H., Rahman, N. H. A., Aris, M. A., Jamaluddin, M. H., Kong Cheh Lin, I., Jumaat, H., Mohd Redzwan, F. N., & Yamada, Y. (2021). Development of C-Shaped Parasitic MIMO Antennas for Mutual Coupling Reduction. Electronics, 10(19), 2431. https://doi.org/10.3390/electronics10192431

[10] A. Kumar, M. Kumar, and A. K. Singh, "Substrate Integrated Waveguide Cavity Backed Wideband Slot Antenna for 5G Applications," *Radioengineering,* vol. 30, no. 3, 2021.

[11] S. Sharma, Mainuddin, B. K. Kanaujia, and M. K. Khandelwal, "Analysis and design of single and dual element bowtie microstrip antenna embedded with planar long wire for 5G wireless applications," *Microwave and Optical Technology Letters,* vol. 62, no. 3, pp. 1281-1290, 2020, doi: https://doi.org/10.1002/mop.32137.

[12] M. A. Khattak, M. I. Khattak, S. M. Owais, A. A. Khattak, and A. Sultan, "Design and analysis of millimeter wave dielectric resonator antenna for 5G wireless communication systems," *Progress In Electromagnetics Research C,* vol. 98, pp. 239-255, 2020.

[13] N. Nasir, M. H. Jamaluddin, N. H. Shahadan, S. M. Abbas, and H. Ahmad, "Compact Substrate Integrated Waveguide Cubical Dielectric Resonator Antenna for fifth-generation applications," *AEU - International Journal of Electronics and Communications,* vol. 187, p. 155551, 2024/12/01/ 2024, doi: https://doi.org/10.1016/j.aeue.2024.155551.

[14] E. Baldazzi *et al.*, "A High-Gain Dielectric Resonator Antenna With Plastic-Based Conical Horn for Millimeter-Wave Applications," *IEEE Antennas and Wireless Propagation Letters,* vol. 19, no. 6, pp. 949-953, 2020, doi: 10.1109/lawp.2020.2984565.

[15] K. T. Lo and H. Wong, "Wideband Millimetre-Wave Dielectric Resonator Antenna Fed by a Wide Aperture," *IEEE Access,* vol. 12, pp. 14521-14531, 2024, doi: 10.1109/ACCESS.2024.3355953.

[16] A. Gorai, A. Deb, J. Panda, and R. Ghatak, "Millimeter Wave/5G Multiband SIW Antenna with Metasurface Loading for Circular Polarization and Bandwidth Enhancement," *Journal of Infrared, Millimeter, and Terahertz Waves,* vol. 43, pp. 1-18, 05/31 2022, doi: 10.1007/s10762-022-00858-2.

[17] K. Wu, M. Bozzi, and N. J. G. Fonseca, "Substrate Integrated Transmission Lines: Review and Applications," *IEEE Journal of Microwaves,* vol. 1, no. 1, pp. 345-363, 2021, doi: 10.1109/JMW.2020.3034379.

[18] A. Alam, M. S. Alam, K. AlMuhanna, and A. Shamim, "A critical review of interconnect options for SIW technologies," *Authorea Preprints,* 2024.

[19] B. Mukherjee, P. Patel, and J. Mukherjee, "A review of the recent advances in dielectric resonator antennas," *Journal of Electromagnetic Waves and Applications,* vol. 34, no. 9, pp. 1095-1158, 2020/06/12 2020, doi: 10.1080/09205071.2020.1744484.

[20] K. M. L. a. K.W.Leung, *Dielectric Resonator Antennas* (Bal dock, U.K.: Research Studies Press). 2003.

[21] L. Kumar, V. Nath, and B. V. R. Reddy, "A wideband substrate integrated waveguide (SIW) antenna using shorted vias for 5G communications," *AEU - International Journal of Electronics and Communications,* vol. 171, p. 154879, 2023/11/01/ 2023, doi: https://doi.org/10.1016/j.aeue.2023.154879.

[22] L. X. Cui, X. H. Ding, W. W. Yang, L. Guo, L. H. Zhou, and J. X. Chen, "Communication Compact Dual-Band Hybrid Dielectric Resonator Antenna for 5G Millimeter-Wave Applications," *IEEE Transactions on Antennas and Propagation,* vol. 71, no. 1, pp. 1005-1010, 2023, doi: 10.1109/TAP.2022.3211389.

[23] X. Liu, X. Wang, G.-M. Yang, D. Xiang, and L.-R. Zheng, "Dual-band frequency reconfigurable metasurface antenna for millimeter wave joint communication and radar sensing systems," *Opt. Express,* vol. 32, no. 8, pp. 13851-13863, 2024/04/08 2024, doi: 10.1364/OE.522684.

[24] S. Ashraf, J. A. Sheikh, U. Rasool, and Z. A. Bhat, "A low-profile high gain U slotted wide band micro-strip antenna for 5G applications," *International Journal of Electronics,* vol. 110, no. 12, pp. 2265-2281, 2023/12/02 2023, doi: 10.1080/00207217.2022.2140838.

[25] A. Gaya, M. H. Jamaluddin, B. Alali, and A. A. Althuwayb, "A novel wide dual band circularly polarized dielectric resonator antenna for milli meter wave 5G applications," *Alexandria Engineering Journal,* vol. 61, no. 12, pp. 10791-10803, 2022, doi: 10.1016/j.aej.2022.04.025.

[26] B. O. Icmez and C. Kurnaz, "High-Gain Dual-Band Microstrip Antenna for 5G mmWave Applications: Design, Optimization, and Experimental Validation," *Applied Sciences,* vol. 15, no. 7, p. 3993, 2025. [Online]. Available: https://www.mdpi.com/2076-3417/15/7/3993.